

# Centrality control of hadron-nucleus interactions by detection of slow nucleons

Ferenc Siklér

*KFKI Research Institute for Particle and Nuclear Physics, Budapest, Hungary*  
*sikler@rmki.kfki.hu*

March 31, 2003

## Abstract

Slow nucleons emitted during a hadron-nucleus interaction can give information on the centrality, impact parameter of the collision. The aim of this note is to provide the reader with the important characteristics of the slow nucleons, focusing on their spectra, correlations. This study tries to build on evidences, hence more weight is put on experimental results than on models.

## 1 Introduction

High energy hadron-nucleus collisions have a long history and an enormous literature: a very complete review contains more than thousand references [1]. Though studied by many experiments, the main questions are still unsolved, making the subject a still open field.

The terminology of slow particles comes from pioneering emulsion work. The emitted slow particles have been classified according to their grain density left in the detection material: "black" or "gray". They are called in a word "heavy". The lighter-colored particles are concentrated forward and called "shower". These names can be converted to corresponding ranges in  $\beta$ , momentum or energy (Table 1).

name	$\beta$	$p$ [MeV/c]	$E_{kin}$ [MeV]
black	0.25	250	30
gray	0.7	1000	400
shower			

Table 1: Classification of particles produced in hadron-nucleus collisions with the borders of the ranges. Momentum and energy ranges are given for nucleons.

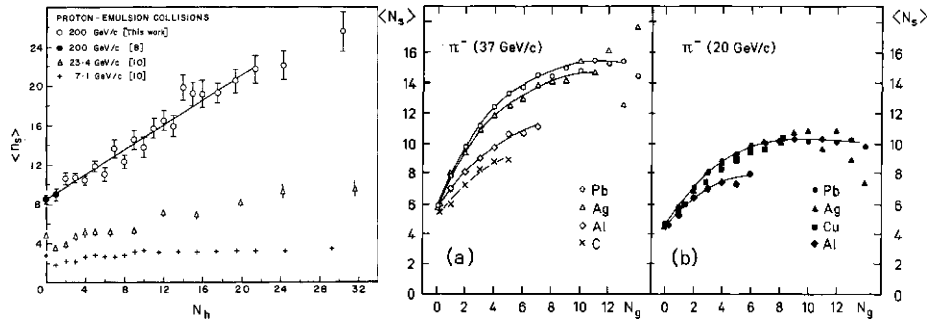


Figure 1: a) Dependence of  $\langle n_s \rangle$  on the number  $N_h$  of heavy particles at 200, 23.4 and 7.1 GeV/c, from Ref. [2]. Line shown is the best linear fit. b) Dependence of the mean number  $\langle N_s \rangle$  of fast particles on the number  $N_g$  of slow particles, from Ref. [3].

## 2 Experimental history

The general observation is that the multiplicities of produced shower particles increase with increasing the number of slow particles: for heavy prongs a closely linear dependence (representative example in Fig. 1a), for grey ones a more curved relation is observed (representative example in Fig. 1b).

The following review is not meant to be exhaustive, but shows the most important steps and developments. The experiments are grouped around measuring techniques, in the end a summary of recent results is given.

Early cosmic ray experiments already indicated that collisions with nuclei produce all kinds of particles: pions, kaons, protons and antiprotons.

### 2.1 Spectrometers

**Cocconi et al.** At the CERN-PS 25 GeV protons interacted with Al and Pt targets [4]. Secondary particles at  $15.9^\circ$  were identified essentially by a mass spectrometer which used magnetic field and the measurement of time of flight between two scintillator counters. The copious production of deuterons and mass-three nuclei was discovered.

**Fitch et al.** Following this line, similar mass analysis was done at Brookhaven AGS by mass analysis of particles emitted from Al and Be targets when struck by 30 and 33 GeV protons [5]. Here several angle settings ( $14\frac{1}{4}^\circ$ ,  $45^\circ$  and  $90^\circ$ ) were used (Fig. 2a). They speculate that most of the  $\pi$  mesons originated in secondary or cascade processes. while low-momentum deuterons could be products of "pick-up".

**Schwarzschild et al.** Another group at Brookhaven AGS performed beam survey at  $30^\circ$  using 30 GeV protons on Al, Be and Fe targets with same technique [6] (Fig. 2b). They state that production of light nuclei involves cooperative phenomena involving several nucleons of the target nucleus, namely by coalescing shower nucleons.

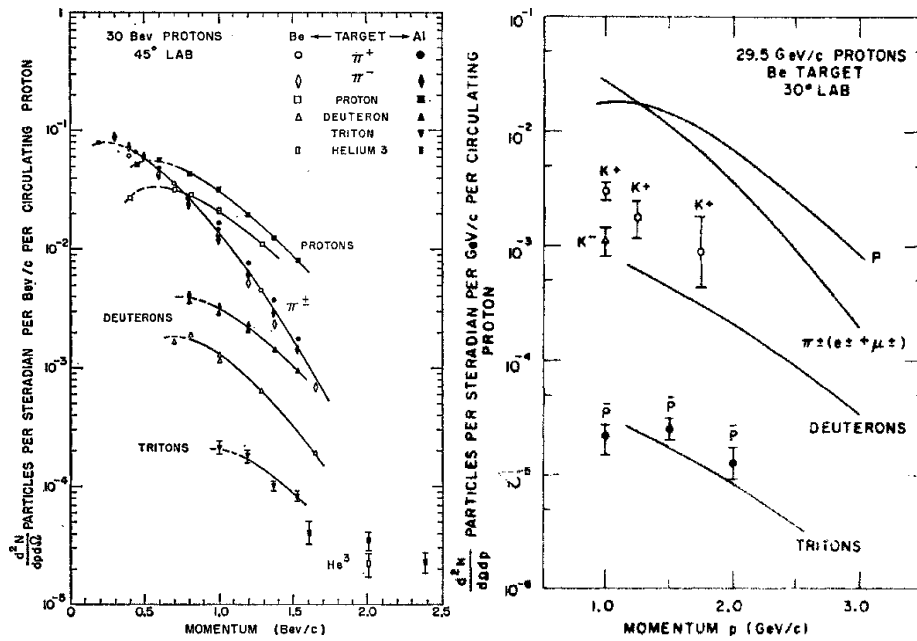


Figure 2: a) Momentum spectra of particles emitted at 45° from Au and Be targets when struck by 30 GeV protons, from Ref. [5]. b) Momentum distribution of particles from Ref. [6].

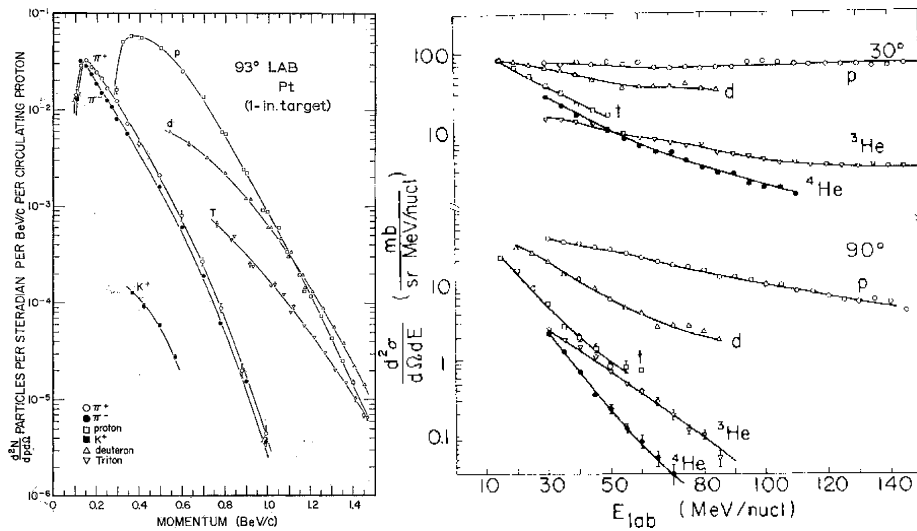


Figure 3: a) Momentum spectra of particles emitted at 93° from Pt target struck by 2.9 GeV protons, from Ref. [7]. b) Double-differential cross-sections for fragments from the irradiation of U by 400 MeV/nucleon  $^{20}\text{Ne}$  ions, from Ref. [8].

**Piroué et al.** Particle production by 2.9 GeV protons on Be and Pt targets have been studied at the Princeton-Pennsylvania Accelerator at various laboratory angles by mass analysis [7] (Fig. 3a). It is found that proton production results both from nucleon-nucleon encounters and processes involving nuclear matter. This latter appears to be necessary to account for observed deuteron, triton, etc., yields.

**Poskanzer et al.** The energy spectra of nuclear fragments produced by the interaction of 5.5 GeV protons with U have been determined at several laboratory angles at Berkeley Bevatron [9]. The measurement was done by means of  $dE/dx - E$  measurements with semiconductor-detector telescopes. By integration angular distributions are obtained and fitted with curves based on the isotropic emission of fragments from a system moving along the beam axis. Being mostly sensitive to black protons the average velocity of the moving system is about  $\beta = 0.006$ .

**Gutbrod et al.** Later particles emitted from U targets irradiated with  $^{20}\text{Ne}$  ions at 400 MeV/nucleon energies were measured with the same method [8] (Fig. 3b). Strong evidence for final-state interactions in the production of high-energy fragments is found. It is suggested that observation of larger composite particles might be a way of selecting central collisions.

**FNAL-E592.** Very complete, high precision measurements of invariant cross-sections for the production of protons, deuterons, tritons,  $^3\text{He}$ ,  $^4\text{He}$ , pions and kaons by 400 GeV protons from a variety of nuclear targets –  $^6\text{Li}$ , Be, C, Al, Cu, Ta – have been performed by the FNAL-E592 collaboration, at angles  $70^\circ$ ,  $90^\circ$ ,  $118^\circ$ ,  $137^\circ$  and  $160^\circ$ , in the momentum range of 0.1 to 1.4 GeV/c [10, 11, 12, 13]. The experiment was performed using independent measurements of the time of flight in the telescope, as well as  $dE/dx$  measurements in the scintillators traversed by the particles. Although they stick to the mere presentation of their data, they note that the empirical function  $\exp(-E_{kin}/E_0)$  is a useful parametrization at a fixed angle (Figs. 4a and 5); there is a clear need for exponential angular dependence of the cross-section on  $\cos\theta$  (Fig. 4b), which arises naturally in several single scattering models via the scaling variable  $E_{kin} - p\cos\theta$ .

## 2.2 Emulsions

**Heckman et al.** Angular and momentum distributions of fragments emitted from central collisions between emulsion nuclei (AgBr) and heavy ion projectiles  $^4\text{He}$ ,  $^{16}\text{O}$  and  $^{40}\text{Ar}$  have been studied at Bevatron-Bevalac at an energy of around 2 GeV/A [14]. Production angles and ranges of fragments having grain density  $g \geq 2g_{min}$  corresponding to protons of  $E < 250$  MeV were measured. The data are successfully fitted and analyzed in terms of a modified Maxwell-Boltzmann distribution (see Sec. 3.4) from which estimates of the longitudinal velocity  $\beta_{||}$  and characteristic spectral velocity  $\beta_0$  of the particle-emitting systems are obtained (Fig. 6a). (It is assumed that the fragments are dominated by one species and the effective Coulomb barrier for emission is small.)

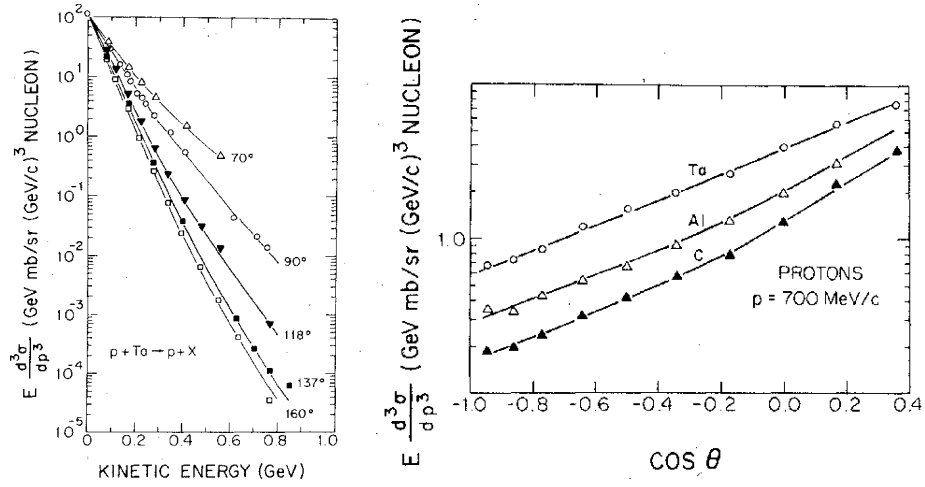


Figure 4: a). Invariant cross-section per nucleon vs kinetic energy at 70°, 90°, 118°, 137°, and 160° (laboratory) for Ta. b) Invariant cross-section per nucleon vs angle at 0.7 GeV/c for C, Al, and Ta. Both from Ref. [11].

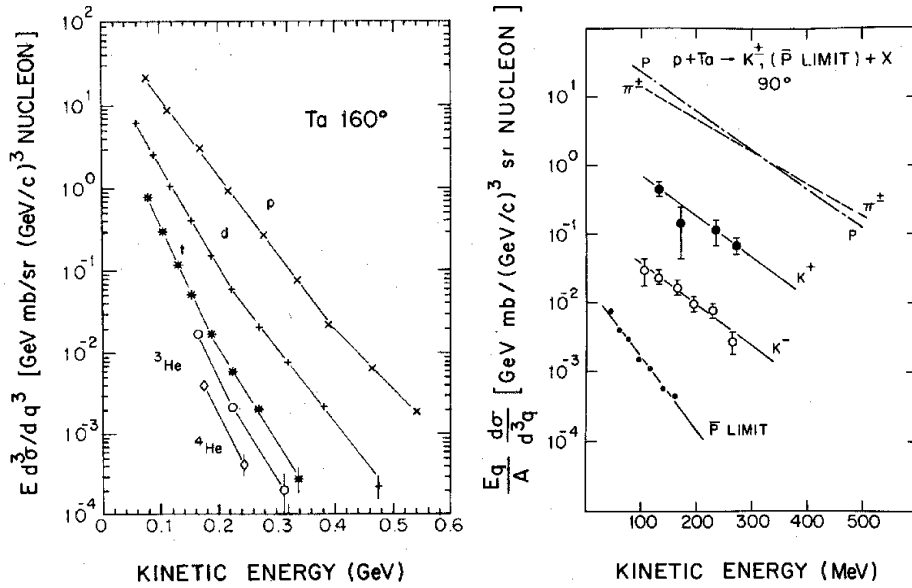


Figure 5: a) Invariant cross-sections per nucleon vs kinetic energy for d, t, <sup>3</sup>He, and <sup>4</sup>He: Ta target at 160° laboratory angle, from Ref. [12]. b) Invariant cross sections per nucleon vs kinetic energy  $T_q$  at 90°, from Ref. [13].

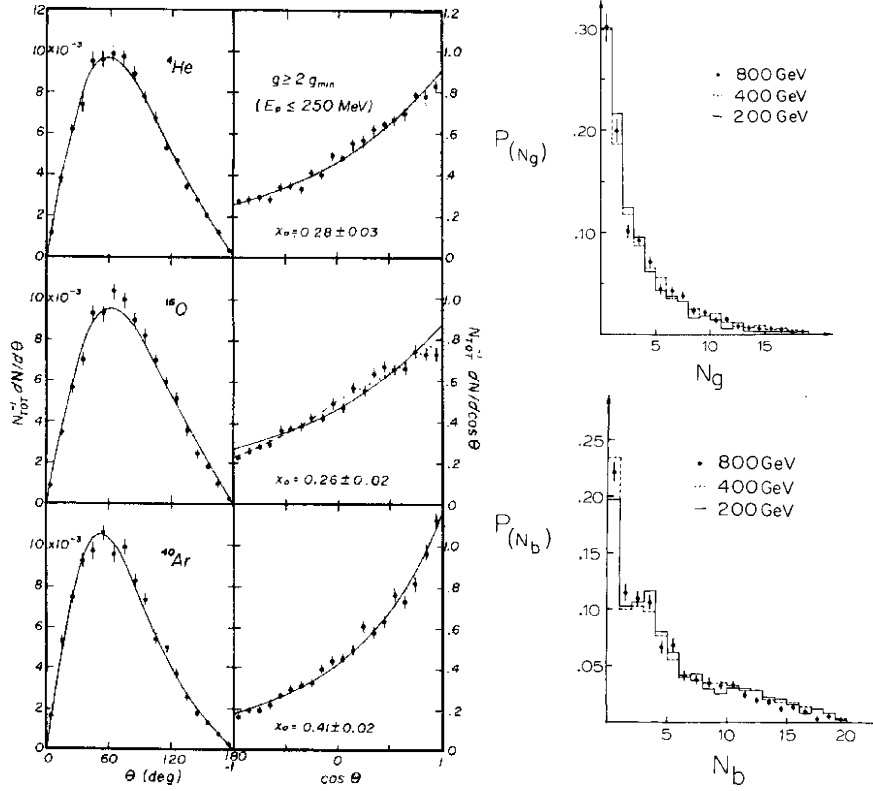


Figure 6: a) Angular distributions for fragments with  $E < 250$  MeV, emitted from central collisions observed in nuclear emulsion, from Ref. [14]. b) Distribution of the number of gray and black tracks in proton-emulsion interactions at 200, 400, and 800 GeV, from Ref. [15].

For the subclass of fragments having  $E < 30$  MeV (black protons) they find that the angular distributions are independent of the mass of the projectile. Longitudinal velocities of the particle-emitting systems are low, typically  $0.014 \pm 0.002$ , other representative experiments showed  $0.01 < \beta_{\parallel} < 0.03$ . The "temperature"  $\tau = m\beta_0^2/2$  is typically 6-7 MeV, independent of projectile.

**Fujioka et al.** Japanese group investigated particles emitted in backward hemisphere with momenta around the kinematic limit of single proton-nucleon collisions, using 205 GeV protons on nuclear emulsion at FNAL [16]. They find that backward pions cannot come from the simple superposition of elementary processes, but may originate from very highly excited states of residual nucleus which took part in the reaction.

**FNAL-E668.** The interaction of 800 GeV protons in nuclear emulsion has been investigated by FNAL-E668 [15]. The distribution of heavily ionizing particles, thus target excitation, is found to be independent of energy when comparing to collisions at 67, 200 and 400 GeV (Fig. 6b). This supports the hypothesis that the number of heavy particles measure the impact parameter

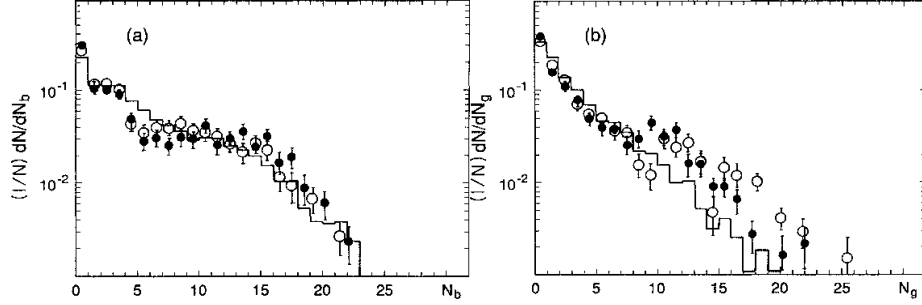


Figure 7: The multiplicity distribution of black and grey tracks for O and S interactions, from Ref. [17].

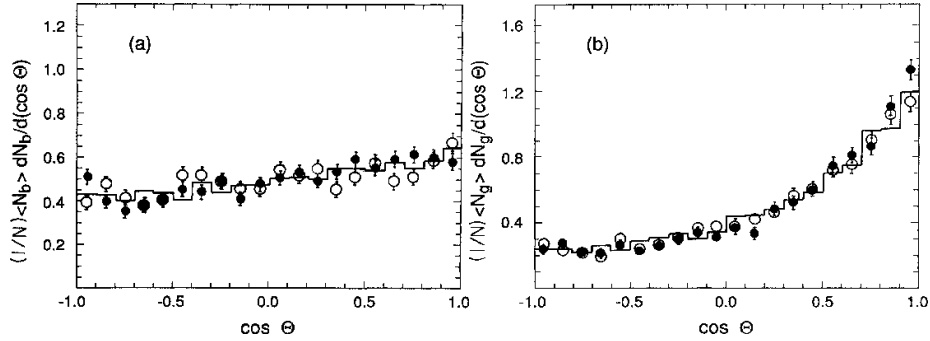


Figure 8: The angular distribution of black and grey tracks from O and S interactions, from Ref. [17]. For comparison the distribution for proton interactions is shown by the histogram.

of the collision and is related to the number of nucleon-nucleon collisions in the target nucleus.

The superposition models assume that each collision of the projectile yields the same distribution of gray particles and that consecutive collisions contribute independently. Hence the angular distribution of gray particles should not depend on primary energy or the number of collisions  $\nu$ . Their results on angular distributions demonstrate both the energy and  $\nu$  independence.

**CERN-EMU07.** Interactions of O and S nuclei of 200 GeV/A in nuclear emulsion have been observed by CERN-EMU07 experiment (KLM collaboration) [17]. They do not find significant deviations from models, such as Venus, describing the interactions as being the superposition of individual nucleon-nucleon collisions.

The value of the total charge  $Q_F(\theta)$  emitted within the very forward cone of angle  $\theta$  can be measured. When  $\theta$  is chosen such that all spectator protons but only a small number of produced particles are contained,  $Q_F$  measures the total charge carried by the noninteracting projectile nucleons. Comparing experimental probability distributions of  $Q_F$  with predictions from Venus model there is generally good agreement. This justifies the use of Venus model to relate the experimentally measured values with the calculated mean number of

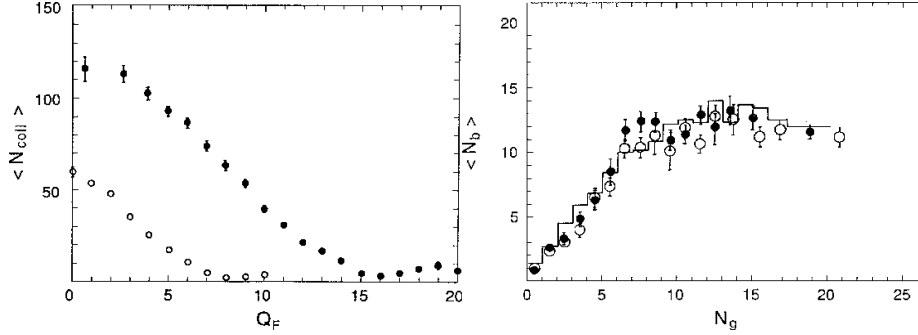


Figure 9: a) The relation derived from the Venus model between the mean number  $\langle N_{coll} \rangle$  of intranuclear collisions and the charge  $Q_F$  for O (open) and S (closed) interactions in emulsion. b) The dependence of the mean number  $\langle N_b \rangle$  of black tracks on the number  $N_g$  of grey tracks, for O (open) and S (closed) interactions in emulsion. For comparison the dependence for proton interactions is shown by the histogram. Both from Ref. [17].

intranuclear collisions  $\langle N_{coll} \rangle$  (Fig. 9a). The latter represents the centrality of the collision. It is shown that  $\langle N_g \rangle$  increases almost linearly with decreasing  $Q_F$  (increasing centrality of the collision), while the  $\langle N_b \rangle$  value for central collisions becomes constant.

The slight angular dependence for the black tracks suggests that they could be emitted isotropically from a moving frame of reference with the velocity  $\beta = 0.01$  (Figs. 7 and 8). They note that differences in the multiplicity and angular distributions of the grey and black tracks point to their different creation processes: initial interaction and evaporation. The mechanism is independent of the number of collisions  $\nu$ . The correlation between the numbers of black and grey tracks is strong for  $N_g \leq 7$ , but for larger values of  $N_g$ , the mean  $N_b$  levels off at a constant value of 12 (Fig. 9b).

**FNAL-E667.** Inclusive 525 GeV  $\pi^-$  interactions in emulsion have been measured by FNAL-E667 [18]. Mentioning the systematic differences between grey and black track identification using range and ionization measurements, only comparison of the number of heavily ionizing track  $N_h$  is considered. They find that multiplicity distributions of heavy tracks do not vary significantly with the energy of the incoming pion, similarly to proton projectile (Fig. 10a). Saturation is observed when  $\langle N_b \rangle$  is plotted against  $N_g$ , similarly to the experiment described above (Fig. 10b). It appears that same number of gray tracks produces a similar degree of target excitation ( $N_b$ ) independent of the kind of projectile and incident energy. The gray track angular distributions are strongly forward-peaked, while the black ones exhibit little asymmetry (Fig. 11). The distributions do not depend significantly on the type of projectile or its energy. The forward-backward ratios decrease slightly with increasing projectile energy, but this can be due to the uncertainties in track identification. If the typical fragmentation energy per nucleon is  $E_0 \sim 6 - 8$  MeV then  $\beta_{||} \leq 0.01$  for the residual system producing black tracks.



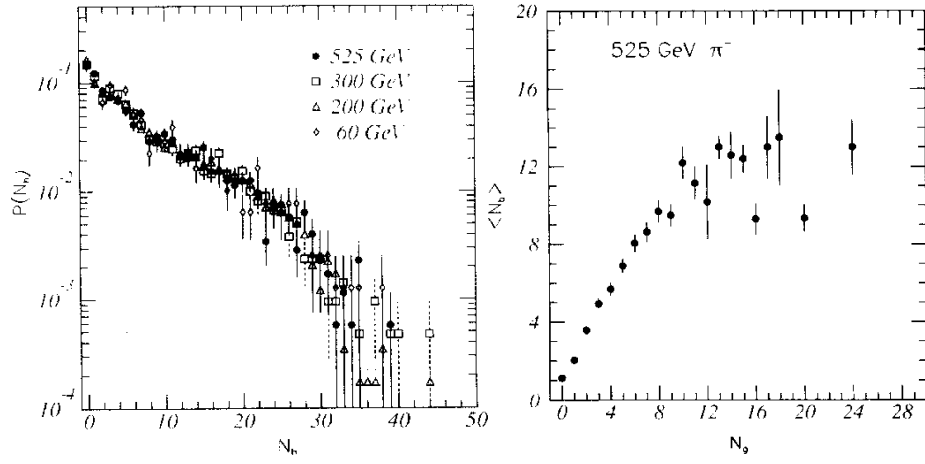


Figure 10: a)  $P(N_h)$  vs  $N_h$  for 60-525 GeV pions. b)  $\langle N_b \rangle$  vs  $N_g$  for 200 GeV  $\pi^-$  and p and 200 GeV/nucleon  $^{16}\text{O}$  and  $^{32}\text{S}$  interactions. Both from Ref. [18].

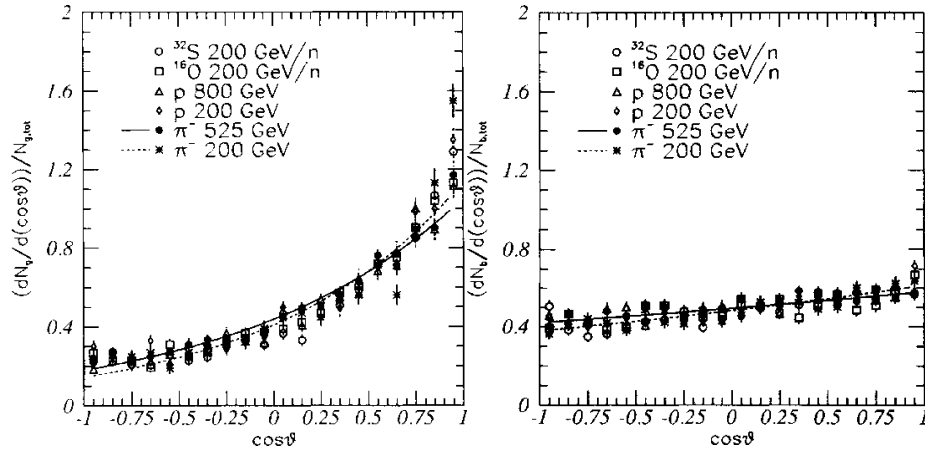


Figure 11: a). Angular distribution of grey tracks for  $\pi^-$ , p and heavy ion interactions in emulsion. Smooth curves are fit to the two-step vector model. b) Same for black protons. Both from Ref. [18].

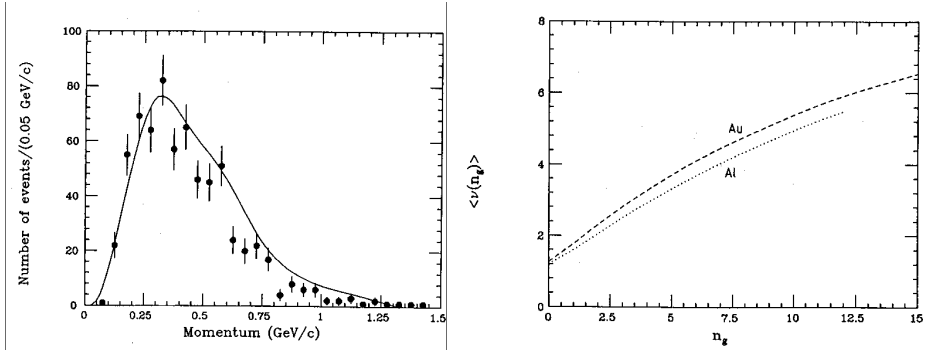


Figure 12: a) Grey tracks momentum distribution. The solid curve gives the prediction of the multi-chain model. b) Average number of collisions between the incident protons and the target nuclei as a function of the number of grey tracks calculated by the multi-chain model. Both from Ref. [22].

### 2.3 Bubble chambers

**Yeager et al.** Detailed studies of  $\pi^+$ Ne and  $\pi^-$ Ne interactions at 10.5 GeV/c have been carried out at SLAC, using bubble chamber [19]. Curvature, range and track density information have been used to separate pions from protons, plus the help of isospin symmetry to untangle the ambiguities. The enhancement of pion production in the target-fragmentation region arises mainly from events with large values of  $N_h$  heavy tracks.  $N_h$  appears to be the measure of the number of struck nucleons inside the nucleus.

**Hayashino et al.** Protons and pions emitted in the backward hemisphere in collisions of 28.5 GeV/c protons with Ta have been studied using hydrogen bubble chamber at BNL [20]. The kind of particles was identified by the usual method from ionization and momentum. Longitudinal momentum distributions show that protons and pions have different average momenta, thus the contribution from isobar decay is small. On the other hand kinetic energy spectra of both particles can be expressed by simple exponential form, suggesting that they come from some kind of thermodynamically equilibrium-like state. Similar results have been obtained using 12.6 GeV/c  $K^-$  beam [21].

**CERN-EHS.** Interactions of 360 GeV/c protons with Al and Au targets were studied using the European Hybrid Spectrometer equipped with the rapid cycling bubble chamber at CERN [22] and compared with calculations based on the multi-chain and Lund models (Fig. 12). The former is in good agreement with data, while the latter is not, probably because it does not include cascading.

The multi-chain model assumes that at each collision the projectile loses a fraction of its momentum according to a probability, and a hadronic chain is stretched between the projectile and the target nucleon. The projectile finally fragments into hadrons, the hadronic chain also hadronizes into pions and the recoil nucleon. The hadrons may come on-shell only after a characteristic formation time (formation zone concept). The model can predict the average number of collisions  $\langle \nu \rangle$  and function of the number of knocked out gray particles  $N_g$ .

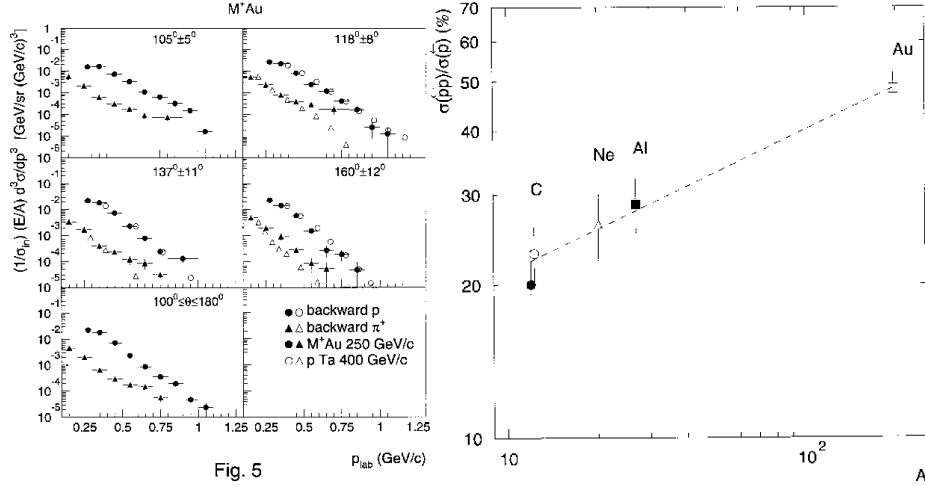


Figure 13: a). The normalized invariant inclusive cross-section per nucleon for backward protons and  $\pi^+$  mesons in different angular ranges, as a function of  $p_{lab}$ , for  $M^+$ Au interactions. b) The contribution of secondary pion absorption to backward proton production, as a function of mass number  $A$ . Both from Ref. [23].

**CERN-NA22.** The same equipment has been used by the CERN-NA22 experiment, studying backward proton production in  $\pi^+$  and  $K^+$  collisions with Al and Au nuclei at 250 GeV/c [23]. Inclusive spectra are in agreement with the higher energy FNAL-E592 results (Fig. 13a). From two-proton correlations it is found that significant part of backward proton production – even as high as 70% for heavy nuclei – can be attributed to secondary pion absorption by a nucleon pair in the nucleus, predicting a low contribution from double color-charge-exchange mechanism (Fig. 13b).

**FNAL-E154.** Multiparticle production in the interactions of 200 GeV/c protons  $\pi^+$  and  $K^+$  mesons with nuclei of Au, Ag and Mg have been studied with bubble-chamber hybrid spectrometer by the FNAL-E154 experiment [24]. Using the net charge  $Q$  of the event and the number of collisions  $\nu$  (obtained via calculation from the number of grey protons), the number of secondary collisions can be calculated. Their results suggest that secondary collisions arise from rescattering of recoiling nucleons rather than produced particles.

**FNAL-E343.** Cumulative particle production in  $p$   $^{20}\text{Ne}$  interactions at 300 GeV have been studied by the FNAL-E343 experiment [25]. Strong correlation between multiplicities of forward- and backward produced protons is observed. The inclusive cross-section for protons can be described by sum of two exponentials plotted as a function of  $p^2$ . The slope is an increasing function of angle (Fig. 14a). Strong signals from  $\Delta$  and  $N^*$  resonances are observed. Evidence for large contribution of cumulative protons from absorption of pions by quasi-two-nucleon systems is found, which can produce up to 40% of all protons emitted backward (Fig. 14b). Comparison with models like additive quark model, Lund

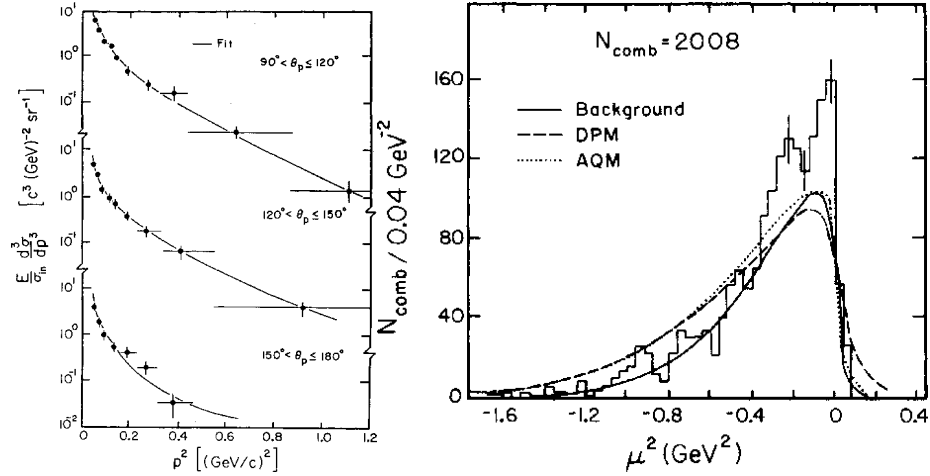


Figure 14: a) The invariant inclusive cross-sections for protons with different angular ranges as function of  $p^2$ . b) The distribution of missing mass square  $\mu^2$  corresponding to the reactions  $\pi + "b" \rightarrow p+p$  and  $\pi + "b" \rightarrow \Delta+p$ . The solid line represents random background. The excess events are from two peaks at  $\mu^2 \sim 0$  and  $\mu^2 \sim -0.22(\text{GeV}/c)^2$ . Both from Ref. [25].

and dual parton model shows that one cannot neglect rescattering (cascading) processes.

## 2.4 Electronic detectors

**CERN-WA35.** Slow particles from collisions of 50, 100 and 150 GeV pions, protons and antiprotons on C, Cu and Pb targets were measured and thoroughly analyzed by CERN-WA35 at the SPS [3, 26, 27]. The slow particles were separated and their energy loss was measured by many CsI scintillator counters covering 52% of the total solid angle, while the forward direction is covered by lucite hodoscope. Angular distributions for higher energy particles are strongly forward peaked, the lower energy ones approach isotropy, reflecting the transition from direct, knock-out protons to thermal ones. Angular distributions show a significant dependence on  $A$ , they are stronger forward-peaked for lighter targets than for heavier ones, while they do not depend on incoming energy (Fig.15).

In their model the incoming projectile collides successively with nucleons moving on a straight trajectory, each recoiling nucleon initiates an internuclear cascade leading to slow nucleons. At a given impact parameter the number of collisions  $\nu$  are assumed to be Poisson-distributed with the mean value obtained from simple Glauber-calculation with Woods-Saxon density distribution. The distribution of slow particles  $N_g$  emitted as result of the cascade is assumed to be Poissonian with mean value fitted to multiplicity distribution. From the model relation between  $\langle \nu \rangle$  and  $N_g$  can be derived (Fig. 16a).

The dependence on projectile type is weaker than predicted by models, in agreement with earlier emulsion experiments (Fig. 16b). This could be cured if recoil nucleons and secondary pions can act as independent hadrons in the

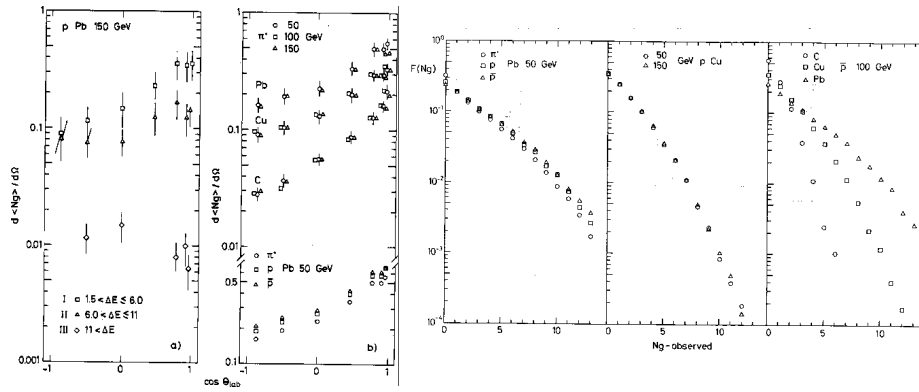


Figure 15: a) Angular distributions of slow particles for different intervals of energy loss,  $\Delta E$  is given in units of the energy loss of minimum ionizing particles. b) Multiplicity distributions of slow particles: projectile, energy and target dependence. Both from Ref. [26].

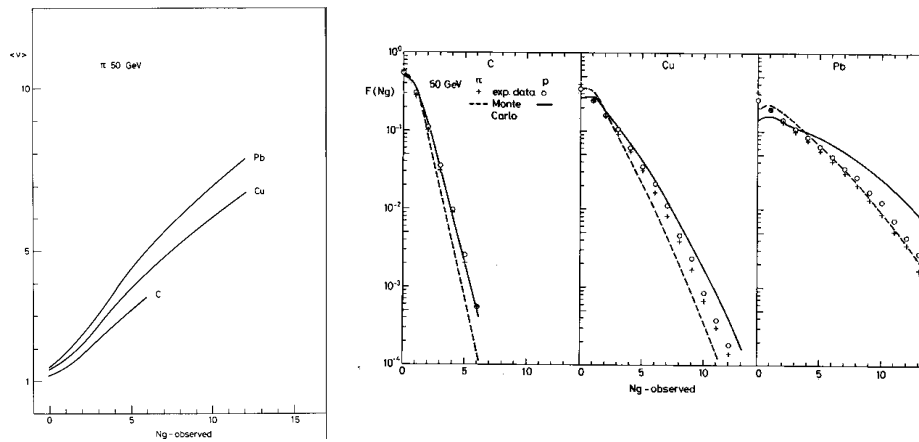


Figure 16: a) The mean number of collisions  $\langle \nu \rangle$  as a function of the number of observed slow particles. b) Comparison of experimental and calculated multiplicity distributions of slow particles for incident pions and protons on C, Cu, and Pb. Both from Ref. [26].

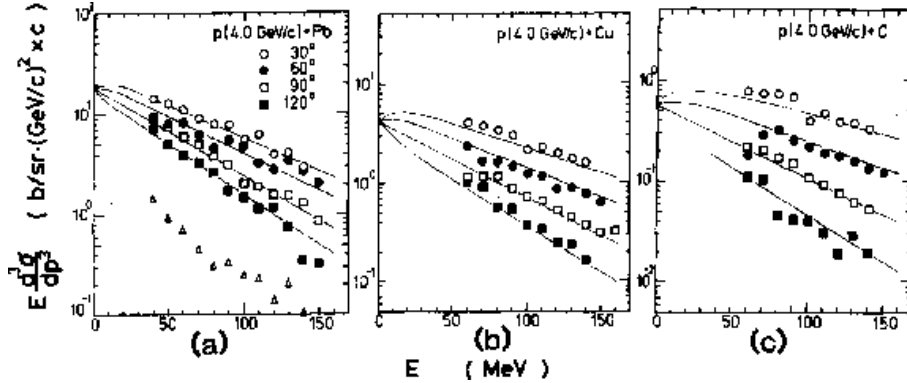


Figure 17: Examples of proton spectra from hadron-nucleus reactions. solid curves are spectra calculated assuming isotropic emissions in a moving frame, from Ref. [28].

nucleus, giving weight to the first collision. The down-stream nucleons which may be hit by projectile are also likely to be hit by the slow particles from the first interaction. For the extreme assumption there could be only one large cascade. It is concluded that the large cascade does not depend directly on the number of primary collisions, but on the average depth of the first interaction and on the remaining thickness of the nucleus at given impact parameter. Hence the number of slow particles would measure the peripherality or centrality of the collision.

**KEK-E90.** Spectra of protons and pions emitted in the target-rapidity region in collisions of 1.5 to 4 GeV/ $c$  pions and protons on C, Cu and Pb targets have been measured with the FANCY spectrometer at KEK [28]. The target was surrounded by a cylindrical multiwire proportional chamber and a trigger hodoscope. Proton spectra were measured using  $\Delta E-E$  scintillation telescopes, calibration was done by time-of-flight measurements. Proton spectra are fitted assuming isotropic emission of protons in a frame moving with a velocity  $\beta_s$  and with a spectrum of  $E d^3\sigma/dp^3 = N_0 \exp(-E/E_0)$ , with good agreement (Fig. 17). The results are consistent with a model of a single-moving-source formation with  $\beta_s = 0.1 - 0.2$  which decays by emitting protons with characteristic energy  $E_0$  of 40 to 70 MeV. While this experiment is sensitive only to the gray proton component, they note that previous measurements observed more low energy components with  $E_0$  parameters 6-9 and 1.5-2 MeV, respectively. From the  $\beta_s$  source velocities the number of nucleons  $\nu$  involved in the formation of the source can be estimated with the relation  $\beta_s = p_{inc}/(E_{inc} + \nu M)$ , where  $M$  is the nucleon mass.

After pushing the momentum acceptance of the detector to a wider range data were fitted with a two-moving-source model, thus introducing an additional, fast source [29] (Figs 18). The parameters obtained are  $E_0 = 50 - 60$  MeV,  $\beta_s = 0.15 - 0.20$  for slow protons,  $E_0 = 125 - 165$  MeV and  $\beta_s = 0.4 - 0.5$  for fast ones. Further analysis concentrated on deuteron data and its understanding with the coalescence model [30].

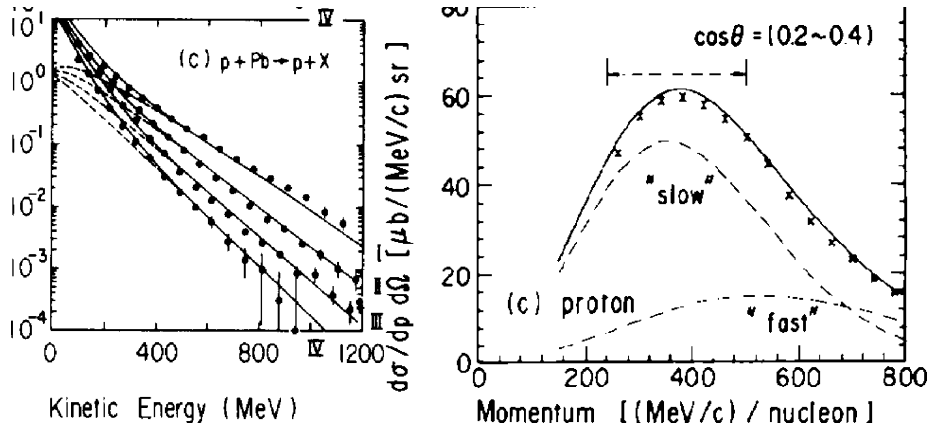


Figure 18: a). Proton spectra emitted in different angular ranges. The fits with the two-moving-source model are shown with the solid line, from Ref. [29]. b) Decomposition of proton spectra with the two-moving-source model, from Ref. [30].

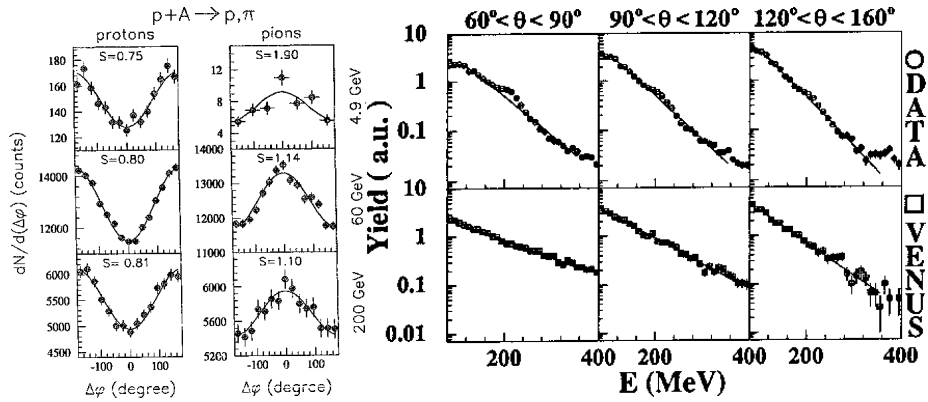


Figure 19: a) The correlation function for p+Au collisions at 4.9 (top), 60 (middle) and 200 (bottom) GeV, from Ref. [31]. b) Energy distributions for p+Au reactions in three different  $\theta$  bins. Data and the Venus model are compared. From Ref. [32].

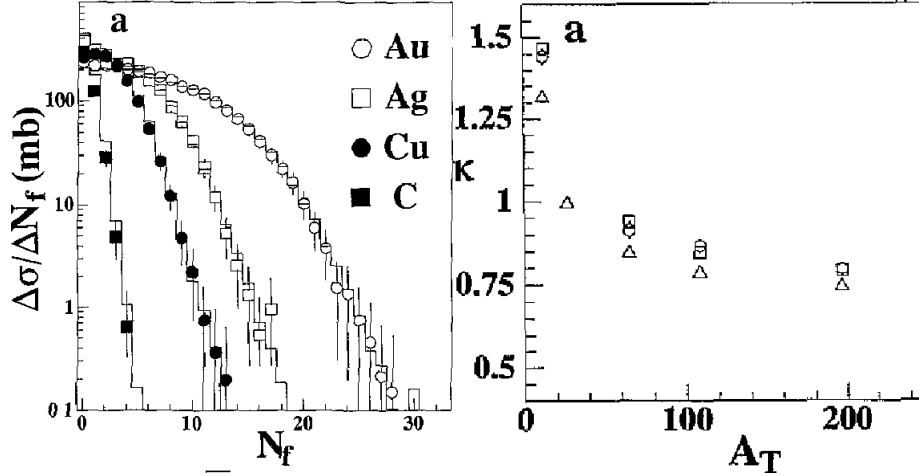


Figure 20: a) Multiplicity distribution of slow fragments in 200 and 60 A GeV  $^{16}\text{O}$  induced reactions on C, Cu, Ag and Au. b)  $\kappa$  dependences in target mass for  $^{16}\text{O}$ -A and p-A collisions. Both from Ref [33].

**CERN-WA80.** Data on proton and pion induced reactions at 60 and 200 GeV/c were taken by the WA80 experiment at CERN SPS with a number of nuclear targets (C, Al, Cu, Ag and Au) [31]. The results were obtained using the Plastic Ball spectrometer which consists of 665 particle identifying telescopes with  $\Delta E - E$  detector, working in the energy range of 30-400 MeV for protons. Comparisons to data taken at 4.9 GeV bombarding energy at the LBL Bevalac with the same detector have been done.

Emitted protons are preferentially back-to-back, while pions are emitted side by side (Fig. 19a). This observation is in accord with pion absorption in the excited target spectator matter. While Venus model fails to describe pions, the RQMD model seems to reproduce data, which might be due to the fact that this one uses experimentally measured cross-sections for  $\pi\text{N}$  reactions, dominated by  $\Delta$  excitation.

For the determination of number-, angular- and energy distributions – in order to achieve essentially background free sample – events with high ( $E_T > 5$  GeV) transverse energy were selected [32]. For the study the geometrical cascade model is adopted. The distribution of number of collisions is calculated using a frozen straight line geometry and a Woods-Saxon potential. Thus number distributions of slow singly charged fragments are fitted with one free parameter, giving a good description. The average number of slow protons produced in an interaction goes like  $\sqrt{A}$  indicating a larger intranuclear cascade.

Neither Fritiof nor Venus produces enough slow protons in comparison with experimental observations. The energy distribution exhibits angular but not target mass dependence. The shape of angular distributions is relatively well described by the form  $\exp(\kappa \cos \theta)$ . The lighter targets have a more forward peaked structure, because they are not large enough for a cascade to become fully developed. Energy distributions are found to have the form of  $\exp(-E/E_0)$  with slope factors 40-60 MeV.

Similar studies have been performed using  $^{16}\text{O}$  projectiles [33] (Fig 20).



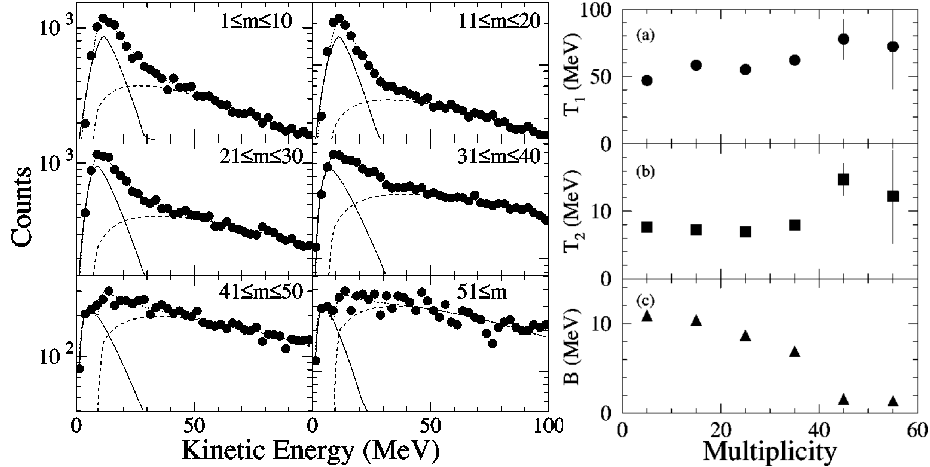


Figure 21: a) Two-stage fit to the proton kinetic energy spectrum for indicated multiplicity intervals. b) Multiplicity dependence of the parameters in the two-stage fit to the proton spectra. Both from Ref. [35].

## 2.5 Streamer chambers

**CERN-NA5.** Interactions of 200 GeV/ $c$  protons on H, Ne, Ar and Xe were studied with a streamer-chamber spectrometer by the CERN-NA5 experiment [34]. Particles were identified based on ionization and the charge of tracks. A rather good identification of knocked out protons in the momentum interval 100 to 600 MeV/ $c$  was achieved.

In the analysis they adopt the geometrical cascade model and calculate the probability distribution of the number of collisions using the Glauber model. They find that the dependence of  $\bar{\nu}$  on number of knocked-out protons is not linear. The dispersion of the centrality measure is also studied.

The number of collisions in the intranuclear cascade is estimated. Each collision brings an extra positive charge when colliding with a proton, or no extra charge when colliding with a neutron. Thus the total number of collisions inside the nucleus is  $\bar{\nu}_{tot} = \langle Q \rangle \frac{A}{Z}$ , where  $\langle Q \rangle$  is the average net charge of all observed secondaries. Having estimated the number of projectile collisions  $\bar{\nu}_p(N_g)$  one can deduce the average number of secondary collisions  $\bar{\nu}_s = \bar{\nu}_{tot} - \bar{\nu}_p$ . It is found that  $\nu_s$  increases rapidly, roughly as  $\nu_p^2$ .

## 2.6 Recent experiments

**LBL-E987.** A high-statistics study of the multifragmentation of 1A GeV Au on C has been performed by LBL-E987 experiment at Bevalac, using the EOS time projection chamber and a multiple sampling ionization chamber [35]. The proton kinetic energy spectra are fitted with sum of two Maxwell-Boltzmann-like functions, one for each of the reaction stages, and studied as function of multiplicity (Fig. 21a). Slope parameters of intranuclear cascade with energetic prompt particles are around 50 MeV, for the emission from an equilibrated system are at about 8 MeV (Fig. 21b).

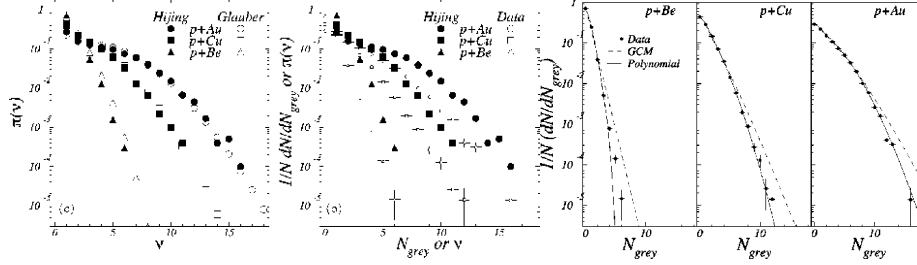


Figure 22: a) Probability distributions for the beam proton to encounter  $\nu$  collisions with target nucleons calculated for p+Be, p+Cu, and p+Au reactions using Glauber and Hijing models. On the right, distributions are overlaid with the  $N_{grey}$  distributions. b) Log-likelihood fits to event normalized  $N_{grey}$  distributions with the geometric cascade and the polynomial model. Both from Ref. [37].

**BNL-E900.** Energy deposition in 5-15 GeV/c proton,  $\pi^-$  and antiproton induced reactions on Au have been studied by experiments BNL-E900 and BNL-E900a at the AGS [36]. Results were obtained with the ISiS silicon sphere  $4\pi$  charge-particle detector array. In order to perform the separation between the thermal-like and nonequilibrium particles, two-component moving source fits, as function of angle, are performed. For the former one source velocity of  $\beta \leq 0.01$  is found.

**BNL-E910.** Slow protons and deuterons from collisions of 18 GeV/c protons with Be, Cu and Au targets have been measured by BNL-E910 experiment at the AGS, performing a detailed analysis of the data [37]. Charged particles were tracked by the EOS time projection chamber in magnetic field supplemented by three drift chambers and time-of-flight walls.<sup>1</sup>

Very detailed studies on the distribution of number of collisions are given by comparing the simple Glauber-calculation to Hijing model (Fig. 22). For the description of number distribution of grey protons a new polynomial model is proposed which incorporates both geometrical and intranuclear cascade models: a strong linear dependence of  $\overline{N}_g$  on  $\nu$  is found. RQMD reproduces distributions and exhibits similar dependence (Fig. 23).

**CERN-NA49.** Hadron-nucleus collisions at 158 GeV/c have been studied by CERN-NA49 experiment [38]. Gray protons have been detected with a gas detector consisting of proportional tubes surrounding the target. Data are compared to known angular distributions and with events from the Venus generator.

**CERN-PS208.** Inclusive neutron spectra were measured by time of flight using 1.22 GeV antiprotons from LEAR on variety of targets – Al, Cu, Ag, Ho, Ta, Au, Pb, Bi and U – by the PS208 experiment at CERN [39]. Sum of two Maxwellian distributions are fitted to the spectra obtained at several angles

<sup>1</sup>The targets were rather thick, 4 mm for the Au, which means that most of slow particles are stopped in the target material. The effect is clearly visible in the momentum distributions and the very steep angular distributions.

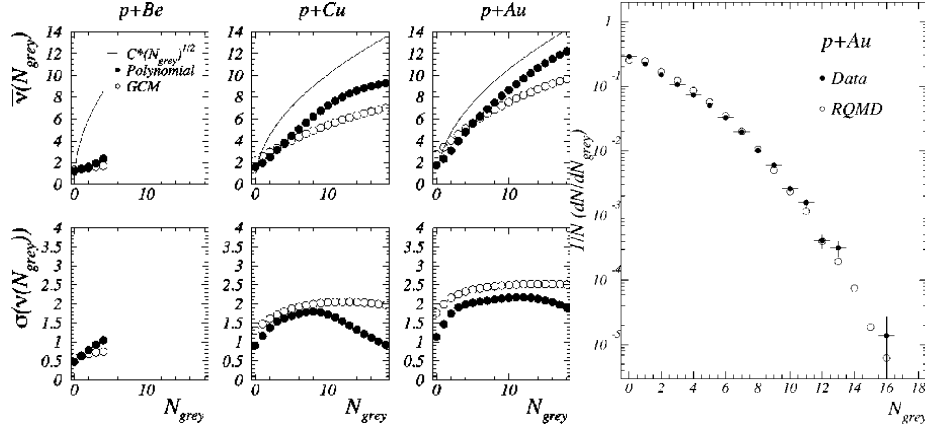


Figure 23: a)  $\bar{v}(N_{grey})$  and  $\sigma$  generated from the polynomial and geometric cascade models and according to the  $\bar{v}^2$  ansatz. b) Comparison between event normalized slow fragment multiplicity distributions for p+Au reactions obtained from data and RQMD calculations. Both from Ref. [37].

yielding total multiplicities and slope for the low-energy evaporative and high-energy pre-equilibrium parts (Fig. 24). While the former component increases with  $A$ , the latter grows with  $A^{1/3}$ , proportional to the nuclear radius. The behavior indicates that the path length of the pions or fast nucleons in the nucleus is responsible for neutron emission. The slope parameters are nearly independent of  $A$ : for all targets the evaporation temperature remains constant around 4 MeV. The slope parameter of the fast neutron spectra is decreasing from Al ( $\approx 48$  MeV) to Ag and then remains constant near 39 MeV for heavier targets (Fig. 25). The agreement with intranuclear cascade calculations is good.

Both neutrons and charged products were detected over a solid angle of  $4\pi$  by means of the neutron ball (spherical tank filled with liquid scintillator, favoring evaporation-like neutrons) and the silicon ball (mostly sensitive to intranuclear cascade products), respectively [40]. Multiplicity distributions of neutrons and protons are given, a good agreement with intranuclear cascade model is found (Fig. 26).

## 3 Models

### 3.1 Number of projectile collisions

**Glauber calculation.** This is the conventional method used by all experiments when presenting their data. At a given parameter  $b$ , the average number of hadron-nucleon collisions is given by the integral

$$\bar{v}(b) = \int_{-\infty}^{\infty} \sigma \rho(z, b) dz \quad (1)$$

where  $\sigma$  is the elementary hadron-nucleon cross-section.

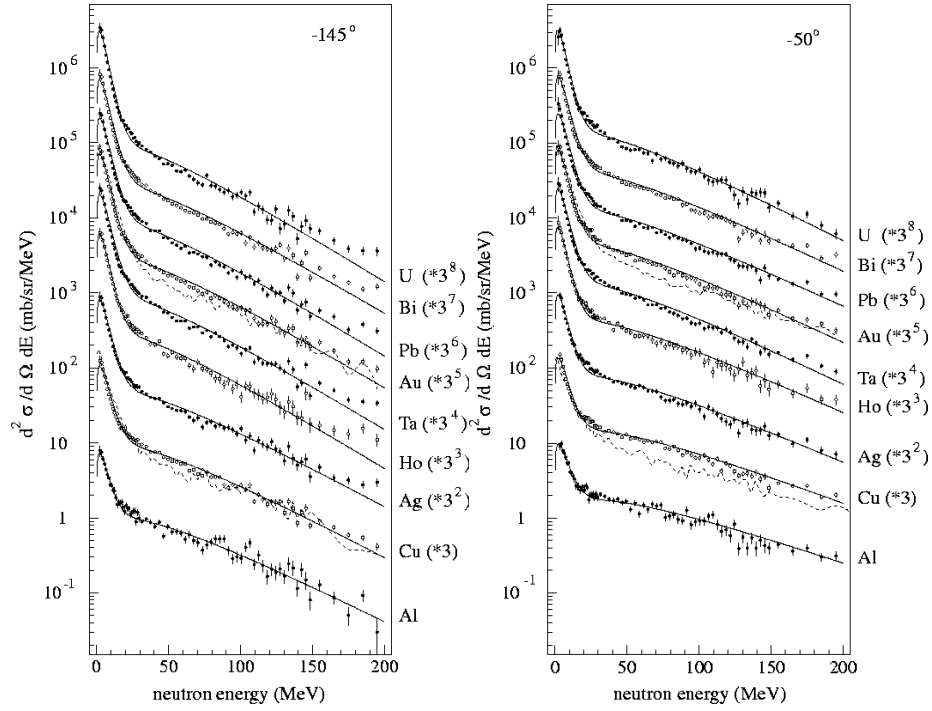


Figure 24: Double differential inclusive neutron production cross-sections vs  $E$  for Al, Cu, Ag, Ho, Ta, Au, Pb, Bi and U targets at emission angles of  $-145^\circ$  and  $-50^\circ$ . Maxwellian fits (solid) and intranuclear calculations (dashed) are also shown, from Ref. [39].

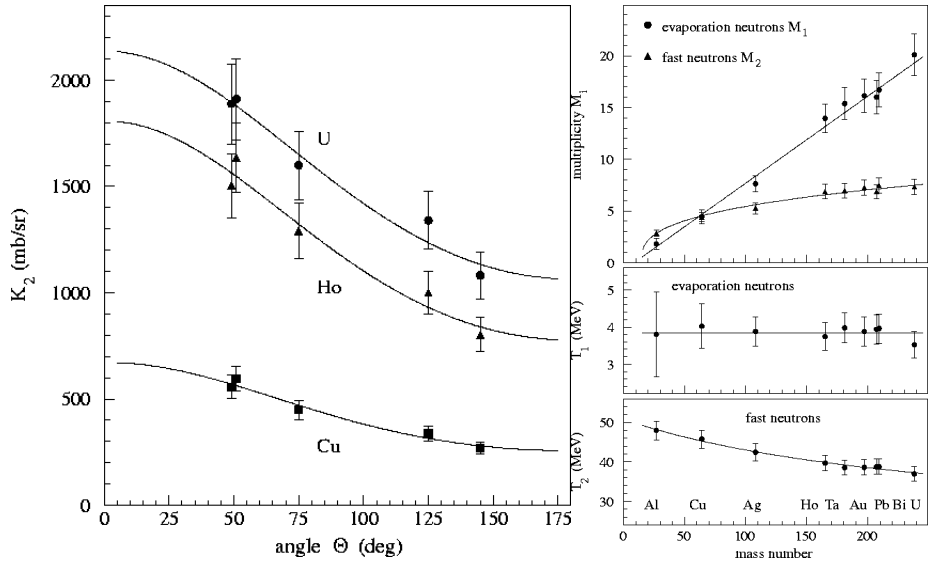


Figure 25: a) Angular distribution of the fast neutrons in Cu, Ho and U targets. b) Target mass dependence of the neutron multiplicities and the inverse slope parameters. Both from Ref. [39].

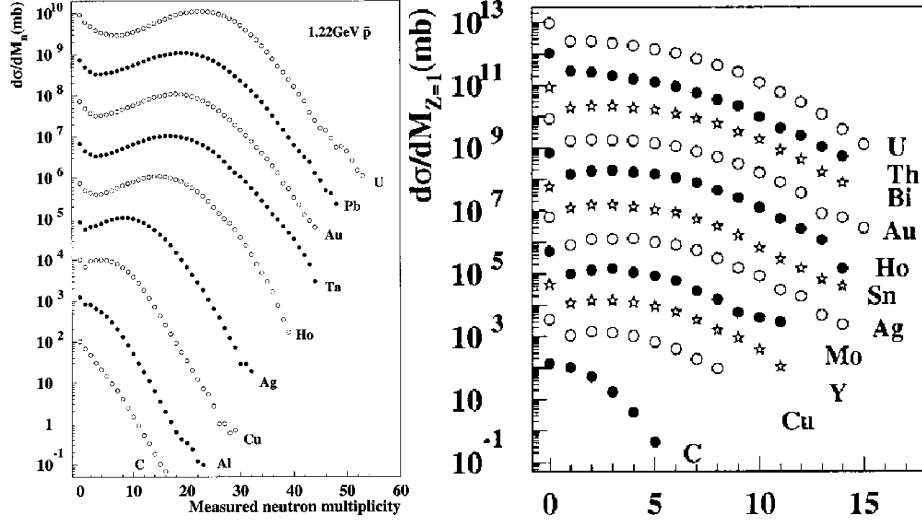


Figure 26: a). Experimental inclusive neutron multiplicity distributions for different targets. The distributions are multiplied by successive factors of 10 for clarity. b) Experimental distributions of multiplicities of  $Z = 1$  particles for different targets (multiplied by successive factors of 10 for clarity). Both from Ref. [40].

For larger nuclei the nuclear density  $\rho$  is often described by a Woods-Saxon distribution in the form

$$\rho(r) = \frac{\rho_0}{1 + e^{\frac{r-R}{a}}} \quad (2)$$

with the mean radius  $R \approx 1.1A^{1/3}\text{fm}$  and the surface diffuseness  $a \approx 0.6\text{fm}$ .

The probability of  $\nu$  collisions for a given impact parameter is assumed to follow a Poisson distribution. (In some variants binomial distribution is used reflecting the finite number of nucleons, maximum thickness, available in the nucleus.) After integration over the impact parameter the probability distribution for number of collisions is obtained,

$$\pi(\nu|b) = \frac{\bar{\nu}(b)^\nu e^{-\bar{\nu}(b)}}{\nu!} \quad \pi(\nu) \propto \int \pi(\nu|b) 2\pi b db \quad (3)$$

**Hijing model.** The distribution  $\pi(\nu)$  was also obtained by experiment BNL-E910 [37] with the Hijing generator which in this context is equivalent to the Lund geometry code. This gives distributions similar to Glauber-calculation.

**Criticism, alternative descriptions.** The validity of assuming sequential projectile-nucleon collisions in the nucleus is already questionable at the energy range ( $E_{lab}$  from 1 GeV to 1 TeV) studied in this note. The collision is so fast that the projectile cannot reach its asymptotic final state, only after having left the nucleus. This also renders the notion of constant hadron-nucleon cross section unsure.

The projectile independence of the distribution of slow nucleons shows that secondary particles acting as independent hadrons can give weight to the first collision (e.g. [26]), in the extreme case producing a single large cascade. Here the production of slow nucleons would measure the *thickness* of the nucleus, thus the peripherality or centrality of the collision and not the number of projectile collisions.

The inelasticity of a hadronic interaction is the fraction of energy not carried off by the fragments of the incoming particle, being available for particle production. The multiple scattering model can be employed to study hadron-nucleus interactions, allowing for changes of the inelasticity of the projectile as it participates in more and more collisions, when passing through the nucleus. The data are fitted using known hadron-nucleon spectra and with the inelasticity as function of collision number. It is found that second and higher interactions of the excited projectile are relatively elastic: they altogether release only 20% (!) of the energy freed in the first collision. The results are checked at SPS energies (e.g. [41]), but there are analyses using high-energy cosmic ray (exceeding  $10^{14}$  eV) cascades with the same conclusion [42, 43]. These findings are thus consistent with "low-energy" data and coincide with the string-type model predictions.

### 3.2 Number distribution of gray nucleons

The analysis is based on the knowledge of two distributions: the distribution of number of projectile collisions in the nucleus  $\pi(\nu)$  and the conditional probability  $P(N_g|\nu)$  of emitting  $N_g$  grey protons in case of  $\nu$  collisions.

The number distribution of grey particles is given by

$$P(N_g) = \sum_{\nu} P(N_g|\nu)\pi(\nu) \quad (4)$$

If  $N_g$  gray particles are emitted the average number of collisions is

$$\bar{\nu}(N_g) = \frac{\sum_{\nu} \nu P(N_g|\nu)\pi(\nu)}{\sum_{\nu} P(N_g|\nu)\pi(\nu)} \quad (5)$$

The accuracy of  $\bar{\nu}$  measurement is limited by the dispersion

$$\sigma = \sqrt{\nu^2(N_g) - \bar{\nu}^2(N_g)} \quad (6)$$

**Geometric cascade model.** According to this simple model, each collision of the incoming hadron in the nucleus corresponds to the same distribution of grey prongs, independent of the projectile [44]. Different encounters give independent contributions. Looking at experimental data showing  $N_g$  distributions at  $\nu = 1$ , for a single encounter a normalized geometric distribution is proposed

$$P(N_g|\nu = 1) = (1 - X)X^{N_g}, \quad X = \frac{\overline{N_g}(\nu = 1)}{1 + \overline{N_g}(\nu = 1)} \quad (7)$$

where the constant  $X$  depends on target nucleus and can be adjusted with a fit to data. From the assumption of independence, for  $\nu$  collisions

$$P(N_g|\nu) = \binom{N_g + \nu - 1}{\nu - 1} (1 - X)^\nu X^{N_g} \quad (8)$$

which is a negative binomial distribution. This also means that

$$\overline{N_g} \propto \overline{\nu} \quad (9)$$

To be able to fit different data sets, it is assumed that the distribution of number of grey prongs is the same whether the incident hadron is a pion or a proton. Furthermore, model imposes no maximum on the number of protons that can be emitted from a nucleus.

**Intranuclear cascade model.** The cascade can also be described from a microscopic point of view [45, 46]. The hadron-nucleus collision is viewed as a sequence of three steps. The hadron passes through the nucleus on an almost straight line and collides with  $\nu$  target nucleons. The struck primary nucleons recoil, travel mostly in forward direction, about half of them detected as grey particles. Their elastic scatterings yield the knocked-out second generation, all of them counted as grey particles. If the primary nucleon is excited they can emit mesons which are too slow and too light to produce grey particles, therefore they are left out of the description. The secondary nucleons collide with other target nucleons to produce the third generation and so on, but they contribute to black tracks and will also be left out.

The following relation for the average number of grey protons can be derived:

$$\overline{N_g} = \frac{Z}{A} \left[ p \langle \nu \rangle + \frac{1}{2} \frac{\sigma_{NN}}{\sigma_{hN}} \overline{\nu(\nu - 1)} \right] \quad (10)$$

Here the first term represents the contribution of the primary protons which will be detected as grey with probability  $p$ . Secondary greys are produced with an effective cross-section  $\sigma_{NN}$ . If a primary nucleon is produced in the  $\mu$ th collision it will scatter  $(\nu - \mu)\sigma_{NN}/\sigma_{hN}$  times before it escapes. Summing up these contributions leads to the second term. Using fits to data [3],  $p = 0.55$  and  $\sigma_{NN} = 29\text{mb}$  is obtained. The two terms can be approximately combined to

$$\overline{N_g} \approx \frac{1}{2} \frac{\sigma_{NN}}{\sigma_{hN}} \frac{Z}{A} \overline{\nu^2} \quad (11)$$

Two fundamental problems are also discussed. While one is usually interested in the number of inelastic collisions, elastic and inelastic hadron-nucleon collisions both lead to recoiling primary nucleons.

After the first inelastic collision the hadron is excited and becomes a different object: its cross-section for the collisions to come may be different from the elementary hadron-nucleon cross-section. (One should note that it is defined for asymptotic states only.) It can be assumed that its cross-section changes continuously along the path: the hadron expands. However from the observation of the grey particles one cannot decide between this description and the usage of a constant effective hadron-nucleon cross-section.

By neglecting the fluctuations in Eq. (11)

$$\overline{\nu}(N_g) \propto \sqrt{N_g} \quad (12)$$

The dispersion of this estimator is proportional to  $\overline{\nu}^{-1/2}$ , thus decreases with increasing number of collisions.

**Polynomial model.** Despite fundamental differences both geometric and intranuclear cascade models successfully reproduce distributions for a number of experiments. A new model is proposed by BNL-E910 experiment [37] that draws elements from both models. The main assumption is that for a given nucleus the mean number of grey tracks  $\overline{N}_g$  is a second order polynomial of the number of primary interactions  $\nu$

$$\overline{N}_g(\nu) = c_0 + c_1\nu + c_2\nu^2 \quad (13)$$

It is further assumed that the distribution is binomial, each target proton can be emitted with probability  $p = \overline{N}_g(\nu)/Z$ ,

$$P(N_g|\nu) = \binom{Z}{N_g} p^{N_g} (1-p)^{Z-N_g} \quad (14)$$

The coefficients  $c_i$  are derived from fits to the data, which show that the quadratic component is negligible and a simple proportionality holds. This is consistent with the geometric cascade model.

### 3.3 Number distribution of black nucleons

Although multifragmentation, breakup of the nucleus is known since cosmic rays physics, it became popular again when it was found to occur in high-energy nuclear reactions. It is a phenomenon involving excitation energies of the order of the nuclear binding energy. In recent years observations pointed to its thermal nature: the remnant undergoes equilibration before breakup. Hence thermodynamic or statistical interpretations should be appropriate (e.g. Refs. [35, 47, 36, 48]). The resulting remnant can be characterized by a few global variables, such as charge, excitation energy and temperature, which may depend on the centrality of the collision.

Due to the above mentioned nature of fragmentation the number distribution of black nucleons can be well described in the form of a binomial distribution,

$$P(n) = \binom{m}{n} p^n (1-p)^{m-n} \quad (15)$$

where  $m$  is the number of available nucleons,  $p$  is the elementary probability, which has the form  $\exp(-B/T)$  with  $B$  being the emission barrier.

One can assume that the average black nucleon multiplicity – hence the target excitation – depends linearly on the number of projectile collisions. This can be deduced from the observation that  $\overline{N}_b$  is proportional to  $N_g$  (Refs. [49, 50, 17, 18]) and from the success of the geometric cascade model which provides the proportionality between  $N_g$  and  $\nu$ . In other words, each collision provides independent and identical production of prompt gray nucleons with identical excitation of the nucleus, leading to the emission of black nucleons.



The saturation of  $\overline{N}_b$  for  $N_g \leq 7$  may simply be the manifestation of the steep distribution of the number of collisions  $\pi(\nu)$ . (Anyway, the region above this is already rarely populated.)

**Average values.** Number distribution of slow nucleons are often presented but almost always subject to biases: the fixed target experiments are mostly insensitive to low energy black nucleons. This makes predictions for the ratio of gray to black nucleons somewhat difficult. A low energy measurement of CERN-PS208 shows that the average multiplicity of grays is 7 and 16 for blacks for Pb nucleus [39], yielding a black/gray ratio of 2.2. According to Refs. [49, 50]  $2.6 \pm 0.1$  gray and  $5.0 \pm 0.2$  black protons have been observed for 200 GeV proton collisions in nuclear emulsion, yielding a ratio of 1.9.

### 3.4 Momentum distribution of slow nucleons

**Modified Maxwell-Boltzmann distribution.** Assuming that the observed system is large enough to be considered statistically, distributions may be parametrised in the form of the Maxwell-Boltzmann distribution <sup>2</sup>: the particles are emitted isotropically, but from a source moving with velocity  $\beta_{\parallel}$ . The invariant cross-section can be written as

$$E \frac{d^3\sigma}{dp^3} \propto \exp(-E_{kin}/E_0) \quad (16)$$

where  $E_{kin}$  is the kinetic energy,  $E_0$  is the characteristic energy per particle, both in the moving system. In the laboratory frame this translates to

$$\frac{dN}{dp d\cos\theta d\phi} \propto \frac{p^2}{\sqrt{p^2 + m^2}} \exp\left[-\frac{\gamma(\sqrt{p^2 + m^2} - \beta_{\parallel} p \cos\theta) - m}{E_0}\right] \quad (17)$$

where  $m$  is the particle mass,  $\theta$  is the laboratory angle between the emitted particle and the initial projectile, the beam direction. Experiments are mostly sensitive to some momentum range only, thus for the angular distribution

$$\frac{dN}{d\cos\theta} \propto \exp(\kappa \cos\theta) \quad \kappa = \frac{\beta_{\parallel} \overline{p}}{E_0} \quad (18)$$

Some results of fits to slow nucleon angular and momentum distributions are given in Table 2. Although the numbers are rather scattered (Fig. 27), an average from the more reliable ones can be drawn.

**Momentum correlations.** Correlation studies show that big part of slow nucleon emission is due to pion absorption in nuclear matter, on quasi two-nucleon-systems (Refs. [25, 31]). This effect may be partially washed out by rescattering.

---

<sup>2</sup>The notion of statistical emission of particles from moving frames is most elaborated at Hagedorn's bootstrap model [51, 52].

	$p_{lab}$ [GeV/c]	$T_b$ [MeV]	$T_g$ [MeV]	$\beta_g$
CERN-PS208	1.22	4	40	0.05
LBL-E987	1	8	50	
KEK-90	3-4		50-60	0.1-0.2
BNL-E900	5-15	10	50	$\leq 0.01$
FNAL-E592	400		45	0.04
"average"		5	50	0.05

Table 2: Result of Maxwellian fits to slow nucleon angular and momentum distributions of several experiments on targets with atomic number close to that of Pb. In the last line a kind of "average" is given, assuming energy independence. (Big weight is given to the precise measurements of CERN-PS208 and FNAL-E592.)

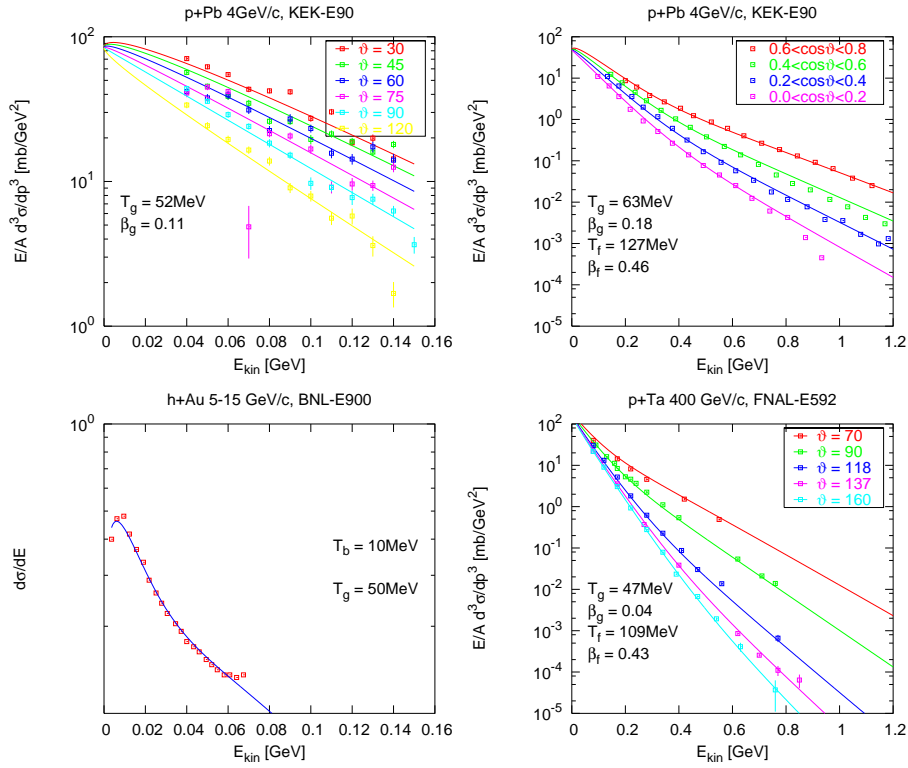


Figure 27: Refits of some of the most complete angle dependent proton cross-sections from collisions of hadrons and heavy nuclei. Sum of Maxwell-Boltzmann distributions were used (b – black, g – gray, f – fast).

## 4 Experimental summary

Although the picture is rather mixed, the important features of the accumulated data in the  $E_{lab}$  range of 1 GeV – 1 TeV can be summarized.

The similarities at different energies suggest the idea that the emission of slow particles is dictated by nuclear geometry, hence supporting the hypothesis of limiting fragmentation.

The data are traditionally analyzed in the framework of the Glauber-model using Woods-Saxon density distribution – providing the distribution of number of projectile collisions in the nucleus  $\pi(\nu)$  – with a model giving the probability distribution of number of slow nucleons  $P(N|\nu)$ . For this latter the usage of the geometric model is most popular.

Based on experimental results the average numbers of black and gray nucleons, in a minimum bias hadron-nucleus collision, are

$$\overline{N}_b \approx 0.08A \qquad \overline{N}_g \approx 1.2A^{1/3} \qquad (19)$$

For centrality selected collisions on Pb target this amounts to

$$\overline{N}_b \approx 4\nu \qquad \overline{N}_g \approx 2\nu \qquad (20)$$

per collision.

Both black and gray components of slow nucleons can be described by independent statistical emission from a moving frame. (It is a bit of surprise for the prompt gray ones where such equilibrated behavior would not be expected.) The number distributions follow binomial distributions.

$$P(N|\nu) = \binom{M}{N} p^N (1-p)^{M-N} \qquad p = \overline{N}/M \qquad (21)$$

where  $M$  is the maximum available protons/neutrons in the nucleus,  $p$  is the emission probability.

The estimation of  $\overline{\nu}$  when detecting  $N$  slow nucleons is given by the projection of the joint  $P(N|\nu)\pi(\nu)$  distribution (see Eq. (5)), its dispersion can also be obtained (see Eq. (6)).

However, one should stress again that experimental observations do not support the analysis described above (see Sec. 3.1). It is often concluded that the production of slow nucleons would measure the *thickness* of the nucleus, thus the peripherality or centrality of the collision and not the number of projectile collisions. Aware of this, one should say that the estimator  $\overline{\nu}(N)$  is a very much model dependent quantity:  $N$  itself could be also employed as a measure of centrality [38].

The momentum distributions are of Maxwell-Boltzmann type with the introduction of a source velocity (see Eq. (17)). While the black nucleons are emitted from a stationary source, the gray nucleons are from a frame moving slowly in the direction of the beam particle (values given for targets with atomic number close to that of Pb):

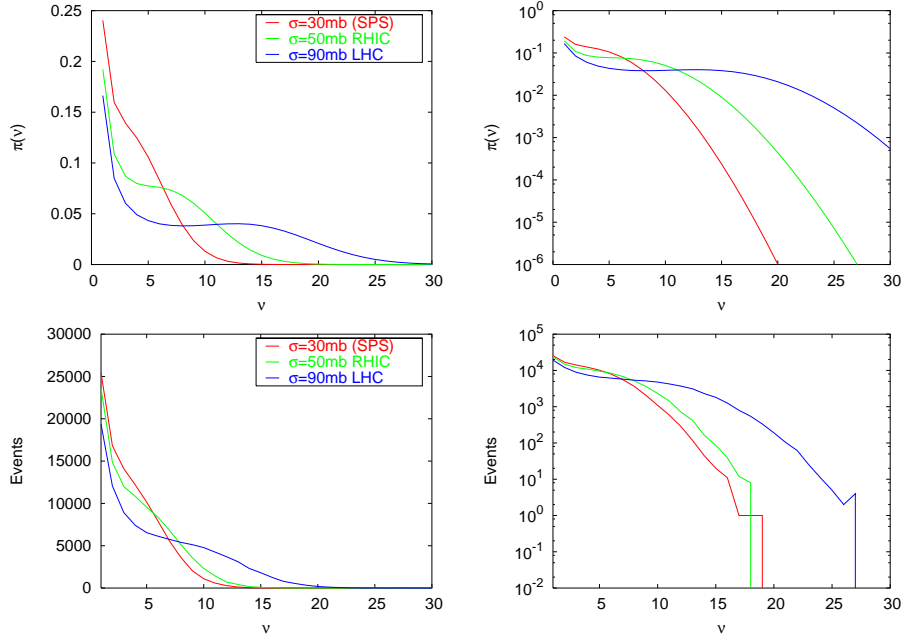


Figure 28: Probability distribution of number of projectile collisions in the nucleus at different energies, plotted in both linear (left) and logarithmic (right) scale: upper) using the Glauber-model. lower) using  $10^5$  events from the Hijing generator, for the three accelerator energies.

$$\beta_b = 0 \qquad \beta_g = 0.05 \qquad (22)$$

$$T_b = 5 \text{ MeV} \qquad T_g = 50 \text{ MeV} \qquad (23)$$

The values of  $\beta$  decrease with increasing  $A$ : for bigger nuclei the intranuclear cascade can develop more, yielding a more isotropic emission of particles.

Some experiments find another very fast components which can be identified with central production or particle emission associated with the projectile hadron.

## 5 Predictions for colliders

The detection of slow nucleons is possible with the zero degree calorimeters (ZDCs), originally planned to measure centrality of nucleus-nucleus collisions. If the proton ZDC is segmented, the black and gray protons can be detected separately, because of the different velocities of frames they are emitted from. Otherwise – and for the neutrons – only the sum of them, the number of ”heavy” particles can be measured.

Heavier nuclei are expected to go down undetected in the beam pipe. Light nuclei can already make hits in the proton ZDC, mostly  $Z/A=2/3$  ( $^3\text{He}$ ) and partly  $Z/A=1/2$  ( $\text{d}, ^4\text{He}$ ) should be considered. They can be produced by repeated coalescence of prompt gray protons and neutrons. In this case the even-

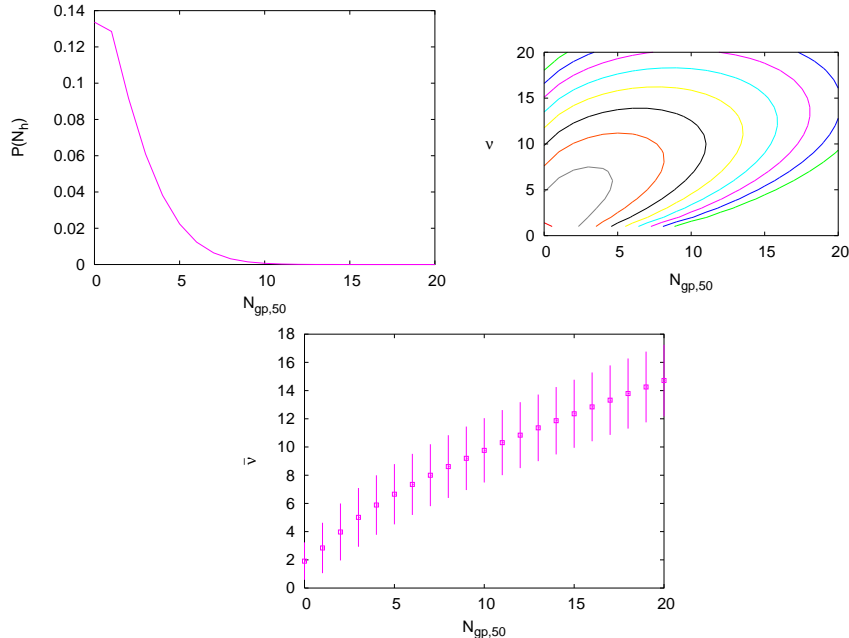


Figure 29: a) Number distribution of gray protons  $N_{gp,50}$  assuming 50% detection efficiency at SPS energy. b) Contour plots of  $N_{gp,50}$  vs  $\nu$ . Each contours are separated by factors of 10. c) The  $\bar{\nu}$  estimator: projection of the joint distribution with the errorbars indicating the resolution.

tual detection of these nuclei (mostly deuterons with some  $^3\text{He}$ ) means just the hit of a few gray nucleons at the same time. However, most of the light nuclei are the products of the late phase of the interaction: evaporation, fragmentation of the nucleus (mostly  $^4\text{He}$  [35]). They can be treated as black nuclei, reporting on the excitation of the nucleus just like black nucleons.

For planning a collider experiment the good knowledge of the momentum distribution of the emitted particles is crucial, due to the presence of a big Lorentz-boost. Data on hadron-nucleus interactions are exclusively available from fixed target experiments. This is why one has to concentrate on results where detailed angle dependent momentum/energy spectra of slow nucleons have been obtained.

The features of the produced slow particles are highly energy independent, they are very similar in the range of projectile energy from 1 GeV to 1 TeV. This applies to angular, momentum and number distributions as well. However it is unclear whether this behavior still holds at collider energies (recall the criticism detailed in Sec. 3.1).

Additional complications come about the increase of elementary hadron-nucleon cross-section,  $\sigma_{NN} \approx 50$  mb for RHIC, 90 mb for LHC, compared to 30 mb at SPS. Does this mean that a hadron will have three times more collisions, thus three times more black and gray nucleons, at LHC than at SPS? Is it only geometry which counts, irrespective of the cross-section? These are such open questions which can only be answered after the first results from RHIC are at hand.

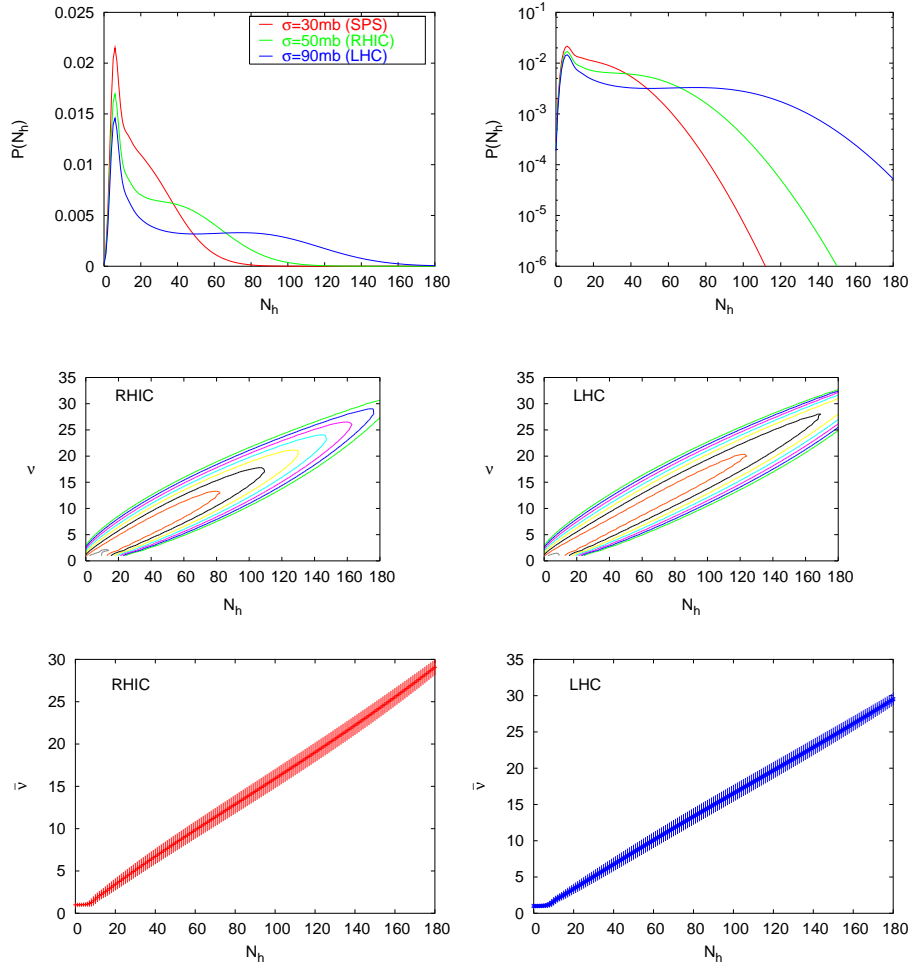


Figure 30: top) Number distribution of slow nucleons  $N_h$  assuming 100% detection efficiency at different energies. middle) Contour plots of  $N_h$  vs  $\nu$ . Each contours are separated by factors of 10. bottom) The  $\bar{\nu}$  estimator: projection of the joint distribution with the errorbars indicating the resolution.

Finally, results of the conventional analysis at SPS, RHIC and LHC energies are shown. The distribution of number of projectile collision is given in Fig. 28, using both Glauber and Hijing model calculations. Experiments where only gray protons are detected with 50% efficiency are shown in Fig. 29 (typical for fixed target). Results where protons and neutrons are detected with 100% efficiency, both black and gray, are given in Fig. 30 (typical for collider). Of course all the plots are highly model dependent.

## Acknowledgments

The author wishes to thank to D. Barna and S. Hegyi for helpful discussions and support. This work was supported by the Hungarian National Science Foundation (F034707) and by the János Bolyai Research Grant.

## References

- [1] S. Fredriksson, G. Eilam, G. Berlad, and L. Bergstrom, Phys. Rept. **144**, 187 (1987).
- [2] A. Gurtu et al., Phys. Lett. **B50**, 391 (1974).
- [3] M. A. Faessler et al., Nucl. Phys. **B157**, 1 (1979).
- [4] V. T. Cocconi et al., Phys. Rev. Lett. **5**, 19 (1960).
- [5] V. L. Fitch, S. L. Meyer, and P. A. Piroué, Phys. Rev. **126**, 1849 (1962).
- [6] A. Schwarzschild and C. Zupančič, Phys. Rev. **129**, 854 (1963).
- [7] P. A. Piroué and A. J. S. Smith, Phys. Rev. **148**, 1315 (1966).
- [8] H. H. Gutbrod et al., Phys. Rev. Lett. **37**, 667 (1976).
- [9] A. M. Poskanzer, G. W. Butler, and E. K. Hyde, Phys. Rev. **C3**, 882 (1971).
- [10] Y. D. Bayukov et al., Phys. Lett. **B85**, 315 (1979a).
- [11] Y. D. Bayukov et al., Phys. Rev. **C20**, 764 (1979b).
- [12] S. Frankel et al., Phys. Rev. **C20**, 2257 (1979).
- [13] N. A. Nikiforov et al., Phys. Rev. **C22**, 700 (1980).
- [14] H. H. Heckman et al., Phys. Rev. **C17**, 1651 (1978).
- [15] A. Abduzhamilov et al. (BATON ROUGE-KRAKOW-MOSCOW-TASHKENT), Phys. Rev. **D39**, 86 (1989).
- [16] G. Fujioka et al., J. Phys. Soc. Jap. **39**, 1131 (1975).
- [17] A. Dabrowska et al. (KLM), Phys. Rev. **D47**, 1751 (1993).
- [18] M. L. Cherry et al., Phys. Rev. **D50**, 4272 (1994).
- [19] W. M. Yeager et al., Phys. Rev. **D16**, 1294 (1977).

- [20] T. Hayashino, O. Kusumoto, G. Fujioka, H. Fukushima, and T. Hara, *Lett. Nuovo Cim.* **16**, 71 (1976).
- [21] H. Fukushima, T. Hayashino, and T. Hara, *Lett. Nuovo Cim.* **21**, 1 (1978).
- [22] J. L. Bailly et al. (EHS-RCBC), *Z. Phys.* **C35**, 301 (1987).
- [23] N. M. Agababian et al. (EHS-NA22), *Z. Phys.* **C66**, 385 (1995).
- [24] D. H. Brick et al., *Phys. Rev.* **D39**, 2484 (1989).
- [25] B. S. Yuldashev et al., *Phys. Rev.* **D46**, 45 (1992).
- [26] K. Braune et al., *Zeit. Phys.* **C13**, 191 (1982).
- [27] K. Braune et al., *Z. Phys.* **C17**, 105 (1983).
- [28] K. Nakai et al., *Phys. Lett.* **B121**, 373 (1983).
- [29] H. Enyo et al., *Phys. Lett.* **B159**, 1 (1985).
- [30] K. Tokushuku et al., *Phys. Lett.* **B235**, 245 (1990).
- [31] H. R. Schmidt et al. (WA80), *Nucl. Phys.* **A544**, 449 (1992).
- [32] R. Albrecht et al., *Z. Phys.* **C57**, 37 (1993a).
- [33] R. Albrecht et al., *Phys. Lett.* **B307**, 269 (1993b).
- [34] C. De Marzo et al., *Phys. Rev.* **D29**, 2476 (1984).
- [35] J. A. Hauger et al. (EOS), *Phys. Rev.* **C57**, 764 (1998).
- [36] T. Lefort et al., *Phys. Rev.* **C64**, 064603 (2001).
- [37] I. Chemakin et al. (E910), *Phys. Rev.* **C60**, 024902 (1999), [nucl-ex/9902003](#).
- [38] S. Afanasiev et al., *Nucl. Instr. Meth.* **A430**, 210 (1999).
- [39] T. von Egidy et al., *Eur. Phys. J.* **A8**, 197 (2000).
- [40] B. Lott et al., *Phys. Rev.* **C63**, 034616 (2001).
- [41] G. M. Frichter, T. K. Gaisser, and T. Stanev, *Phys. Rev.* **D56**, 3135 (1997), [astro-ph/9704061](#).
- [42] G. Wilk and Z. Wlodarczyk, *Phys. Rev.* **D59**, 014025 (1999), [hep-ph/9803435](#).
- [43] C. R. A. Augusto et al., *Phys. Rev.* **D61**, 012003 (2000).
- [44] B. Andersson, I. Otterlund, and E. Stenlund, *Phys. Lett.* **B73**, 343 (1978).
- [45] M. K. Hegab and J. Hufner, *Phys. Lett.* **B105**, 103 (1981).
- [46] M. K. Hegab and J. Hufner, *Nucl. Phys.* **A384**, 353 (1982).
- [47] L. Beaulieu et al., *Phys. Lett.* **B463**, 159 (1999), [nucl-ex/9906012](#).



- [48] L. Beaulieu et al., Phys. Rev. **C64**, 064604 (2001).
- [49] J. Babecki et al., Phys. Lett. **B47**, 268 (1973).
- [50] Z. V. Anzon et al. (ALMA ATA-LENINGRAD-MOSCOW-TASHKENT),  
Yad. Fiz. **22**, 736 (1975).
- [51] R. Hagedorn, Nuovo Cim. Suppl. **3**, 147 (1965).
- [52] R. Hagedorn and J. Ranft, Nuovo Cim. Suppl. **6**, 169 (1968).